

Isotope Effects in Dissociative Recombination, in *Dissociative Recombination: Theory, Experiment, and Applications III*, ed. by M. Larsson, J. B. A. Mitchell, and I. Schneider (World Scientific, Singapore, 2000).

ISOTOPE EFFECTS IN DISSOCIATIVE RECOMBINATION

STEVEN L. GUBERMAN

*Institute for Scientific Research, 33 Bedford St., Lexington, MA 02420,
USA*

E-mail: slg@sci.org

The dissociative recombination of $^{18}\text{O}^{16}\text{O}^+$ leading to $\text{O}(^1\text{S})$ is explored with large scale quantum theoretical calculations and compared to the dissociative recombination of $^{16}\text{O}_2^+$. In both cases, the spin-orbit mechanism for mixing the Rydberg states is included in the calculation. At 300K and 1000K, the rate coefficient for $^{18}\text{O}^{16}\text{O}^+$ is larger than that for $^{16}\text{O}_2^+$ by factors of 2.6 and 1.9 respectively. The difference in rate coefficients is shown to be entirely due to indirect recombination. The results show that caution is needed in comparing storage ring derived rate coefficients and quantum yields for different isotopomers and in using storage ring results for $^{18}\text{O}^{16}\text{O}^+$ in environments where the dominant isotopomer is $^{16}\text{O}_2^+$.

1 Introduction

A difficulty with the interpretation of some of the early experimental studies of dissociative recombination (DR) was the unknown vibrational (and occasionally electronic) distribution of the ion undergoing recombination. The DR rate coefficient can be quite sensitive to the ion vibrational or electronic distribution. One of the advantages for using storage rings to study DR is the opportunity to hold a molecular ion in the ring for enough time to allow electronic and vibrational relaxation to occur by photon emission. This strategy works well for many heteronuclear diatomic ions but does not work for homonuclear ions such as N_2^+ and O_2^+ where the decay times are much too long. A way around this problem is to use isotopomers such as $^{15}\text{N}^{14}\text{N}^+$ [1] and $^{18}\text{O}^{16}\text{O}^+$ [2]. These species have nonzero dipole moments allowing for some relaxation of the ion vibrational distribution before recombination. A question that arises in these studies is: Are the results of these storage ring experiments applicable to $^{14}\text{N}_2^+$ and $^{16}\text{O}_2^+$ or are the results only meaningful for the studied isotopomer? Below, we explore this issue with theoretical calculations of the DR of $^{16}\text{O}_2^+$ and $^{18}\text{O}^{16}\text{O}^+$ leading to $\text{O}(^1\text{S})$. Section 2 has a description of the theoretical approach. Section 3, has a review of the spin-orbit coupling DR mechanism for this process. The theoretical calculations on the isotopomers are described in Section 4 and the conclusions are in Section 5.

2 Methods

The potential curves discussed here have all been calculated using large scale wave functions in [5s, 4p, 3d, 2f, 1g] [3] basis sets [4]. The molecular orbitals are determined in Complete Active Space Self Consistent Field (CASSCF) [5] calculations involving all electronic excitations in the space of the valence orbitals. From the orbitals, a configuration interaction (CI) [6] wave function is determined in which all single and double electronic excitations are taken from the CASSCF configurations to the full virtual space of the remaining orbitals that are not in the CASSCF. All potential curves have been calculated with the MOLPRO programs [7]. The next section has a brief review of the spin-orbit mechanism for generating $O(^1S)$ from the DR of O_2^+ . The mechanism uses both $^3\Sigma_u^-$ and $^1\Sigma_u^+$ repulsive potential curves. For $^3\Sigma_u^-$, the spectroscopic constants are well known. The calculated (experimental)[8] spectroscopic constants are 721.0 (709.057) cm^{-1} for ω_e , 13.0 (10.61408) cm^{-1} for $\omega_e x_e$, 3.0311 (3.03165) a_0 for R_e and 6.2379 (6.1737) eV for T_e . The accurate calculated values for R_e and T_e give us confidence that the rate coefficients calculated with these potential curves will also be accurate. The rate coefficients reported here use an improved description of the repulsive wall of the $^3\Sigma_u^-$ and $^1\Sigma_u^+$ dissociative states and the results differ slightly from those reported previously [12]. Further details of these calculations will be reported separately [9a].

For the electronic widths, high Rydberg orbitals have been used to represent the free electron continuum orbital using an approach described previously [9b, 11].

For the cross sections and rate coefficients, we have used the Multichannel Quantum Defect Theory (MQDT) approach [10, 11] revised to handle the spin-orbit coupling described below.

3 Spin-orbit Coupling Mechanism

The mechanism for generating $O(^1S)$ from the DR of O_2^+ has already been described [12] and the reader is referred to Ref. 12 for more details. The mechanism is illustrated in Fig. 1. The two repulsive potential curves shown, $^1\Sigma_u^+$ and $^3\Sigma_u^-$, dissociate to $O(^1S) + O(^1D)$ and $O(^3P) + O(^1D)$ respectively. $^1\Sigma_u^+$ is the only state that can generate $O(^1S)$ from the ion vibrational levels shown in Fig. 1. At first glance, you may be wondering why a state that does not dissociate to $O(^1S)$ would have anything to do with the production of $O(^1S)$ by DR. Indeed, as we shall see shortly, the $^3\Sigma_u^-$ state is of paramount importance to this mechanism.

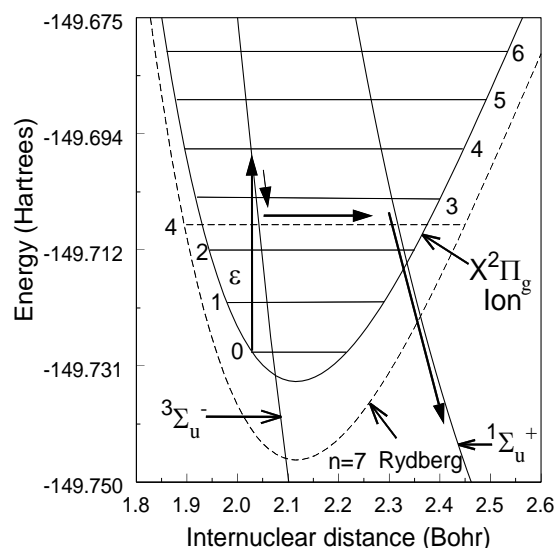


Figure 1. Repulsive, Rydberg, and ion potential curves for the DR of O_2^+ .

Capture of an electron of energy ε (see Fig. 1) from the $v=0$ ion level can occur into either repulsive state. Because of its favorable crossing within the turning points of the ion $v=0$ level, the Franck-Condon factor between the ${}^3\Sigma_u^-$ vibrational wave function and the ion $v=0$ wave function is much larger than that for ${}^1\Sigma_u^+$. If we ignore the ${}^3\Sigma_u^-$ state [11], the calculated quantum yield for $O(^1S)$ is only 0.0012, i.e. for every pair of atoms produced in DR, only 0.0012 atoms will be $O(^1S)$.

Also shown in Fig. 1 is the potential curve for a Rydberg state with a principal quantum number, n , of 7. Note that this curve does not have an electronic symmetry label. The reason will be apparent shortly. In the MQDT approach and in all prior calculations of DR cross sections that include indirect [13] recombination through the intermediate Rydberg levels, the Rydberg states are always of the same electronic symmetry as the dissociative states. These Rydberg states are predissociated by the repulsive curves because there is a nonzero predissociation matrix element (over the electronic Hamiltonian) between both states. The electronic Hamiltonian matrix elements between states of different electronic symmetry are zero. However, there are small nonzero matrix elements between states of different electronic symmetry over operators that describe higher order effects. Because these matrix elements are small, they have been neglected in all prior theoretical studies of DR. For the potential curves of Fig. 1, the rate coefficient

for DR from $v=0$ through only $^1\Sigma_u^+$ is so small (2.3×10^{-10} cm³/sec at 300 K [11]) that any small increase in the flux exiting through the $^1\Sigma_u^+$ channel can have a significant effect upon the magnitude of the O(¹S) quantum yield. The exiting flux along $^1\Sigma_u^+$ can be increased if there is a pathway to $^1\Sigma_u^+$ for some of the flux that is initially captured in other dissociative channels. Consideration of the spin-orbit coupling operator matrix elements and of the electronic symmetries of the other channels [14] that are DR routes for the low vibrational levels of O₂⁺ shows that the only other symmetry that can interact with $^1\Sigma_u^+$ by spin-orbit coupling is $^3\Sigma_u^-$. The interaction of the dissociative states with each other by spin-orbit coupling is negligible due to the small overlap between the vibrational continuum functions. However, the interaction between the Rydberg states while small is very important. The $^1\Sigma_u^+$ and $^3\Sigma_u^-$ Rydberg states have different quantum defects and are energetically displaced from each other. This displacement decreases as n increases such that by $n=9$, the displacement is only about 12 cm⁻¹. A small interaction will cause these closely spaced high n states to mix with each other. The interaction due to spin-orbit coupling in this case has been determined experimentally to be about 100 cm⁻¹ [15]. This interaction is sufficient to substantially mix the high n $^1\Sigma_u^+$ and $^3\Sigma_u^-$ Rydberg states. The spin-orbit coupling arises from the singly occupied O₂⁺ valence $1\pi_g$ orbital. The spin-orbit interaction splits the ground state of O₂⁺ into a lower $^2\Pi_{1/2g}$ and an upper $^2\Pi_{3/2g}$ state separated by about 200 cm⁻¹. These two states are the limits of the two series of mixed $^1\Sigma_u^+$ and $^3\Sigma_u^-$ Rydberg states.

In the mechanism, as depicted in Fig. 1, an electron is initially captured by $v=0$ into both the $^1\Sigma_u^+$ and $^3\Sigma_u^-$ dissociative states. However, most of the capture is into $^3\Sigma_u^-$ because of its favorable crossing with $v=0$. In addition to dissociation along $^3\Sigma_u^-$ some of the flux enters the mixed symmetry Rydberg states that now connect the $^1\Sigma_u^+$ and $^3\Sigma_u^-$ dissociative states. Some of this flux decays by autoionization, some returns to the $^3\Sigma_u^-$ state and some enters the $^1\Sigma_u^+$ dissociative state and leads to dissociation to O(¹S) and O(¹D). The calculated quantum yield [9a] at room electron and vibrational temperature from the $^2\Pi_{1/2g}$ state is 0.013, i.e. almost a factor of 11 larger than the quantum yield obtained with only the $^1\Sigma_u^+$ state included in the calculation [11].

4 Results

The calculated rate coefficients for DR of the $v=0$ level of the $X^2\Pi_{1/2g}$ state for both $^{16}\text{O}_2^+$ and $^{18}\text{O}^{16}\text{O}^+$ are shown in Fig. 2. The rate coefficient for $^{18}\text{O}^{16}\text{O}^+$ exceeds that for $^{16}\text{O}_2^+$ over the full range of electron temperatures from 100K to 3000K. The rates differ by a factor of about 2.6 at room temperature and by a factor of about 1.9 at

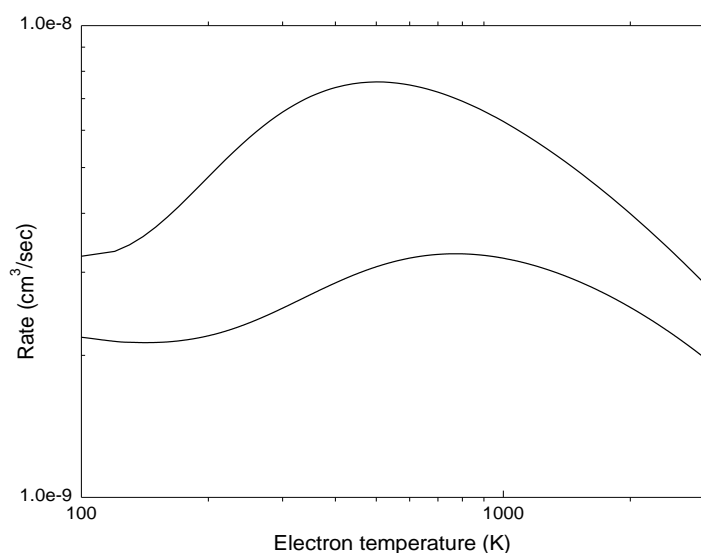


Figure 2. DR rate coefficients for $^{16}\text{O}_2^+$ (lower curve) and $^{18}\text{O}^{16}\text{O}^+$ (upper curve).

1000 K. What is the origin of this isotope effect? In order to explore this further, it is necessary to compare the cross sections, shown in Fig. 3, for the two isotopomers. The cross sections were calculated from 0.0001 eV to 1.0 eV electron energy for capture by $v=0$, $X^2\Pi_{1/2g}$ using 19 vibrational levels in the $X^2\Pi_{1/2g}$, $^2\Pi_{3/2g}$, and Rydberg states [9a, 12]. Below 0.0017 eV, the $^{16}\text{O}_2^+$ cross section exceeds the $^{18}\text{O}^{16}\text{O}^+$ cross section. Above 0.0017 eV, $^{18}\text{O}^{16}\text{O}^+$ is the larger cross section (with some isolated exceptions) and both cross sections show a series of resonances that terminates at 0.0248 eV. These resonances are due to the $v=0$ Rydberg levels that lie between the $v=0$ levels of the $X^2\Pi_{1/2g}$ and $^2\Pi_{3/2g}$ states. These Rydberg states have the $^2\Pi_{3/2g}$ state as core and the lowest energy resonance has $n=24$. Instead of showing an undistorted resonance progression, it is clear that these resonances are affected by different interference in each case. Except for the effects of interference,

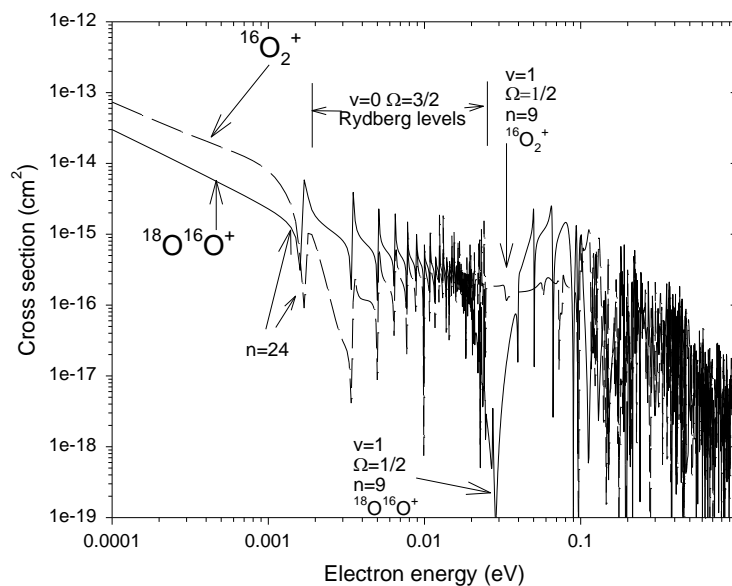


Figure 3. Full DR cross sections for $v=0$ of $X^2\Pi_{1/2g}$ for $^{18}\text{O}^{16}\text{O}^+$ (solid) and $^{16}\text{O}_2^+$ (dashed).

the $v=0$ resonance positions are the same for both isotopomers. The high n Rydberg states have potential curves that are similar to that for the ion, shifted to the appropriate Rydberg energy. The calculated $v=0$ level of $^{18}\text{O}^{16}\text{O}^+$ lies 0.0033 eV below that for $^{16}\text{O}_2^+$. The $v=0$ levels of the high Rydberg states also shift down by 0.0033 eV. As a result, relative to the $v=0$ level of $X^2\Pi_{1/2g}$, the $v=0$ resonances fall at nearly identical energies for the isotopomers. As we shall see shortly, this is not the case for the remaining Rydberg vibrational levels.

At energies above 0.0248 eV and below 0.094 eV, Fig. 3 shows a relatively flat cross section for $^{16}\text{O}_2^+$ with some slight distortion. In the same region, the $^{18}\text{O}^{16}\text{O}^+$ cross section has a pronounced dip at about 0.029-0.027 eV followed by four prominent peaks. The source of these different resonance structures can be identified with some computer “experiments.”

Fig. 4 shows the first computer “experiment” in which the full $^{18}\text{O}^{16}\text{O}^+$ cross section from Fig. 3 is plotted with a cross section calculated with only the $v=0$ Rydberg and ion levels. The cross section with only the $v=0$ levels is mostly below

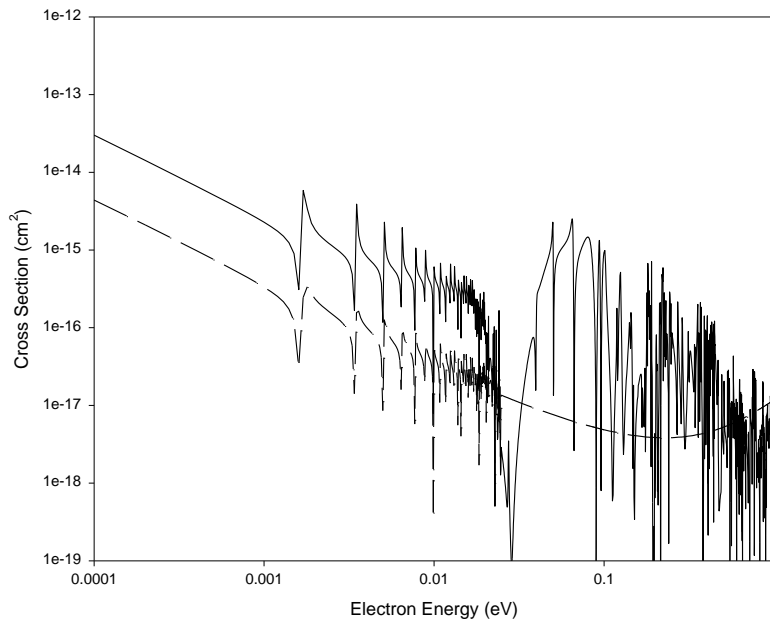


Figure 4. $^{18}\text{O}^{16}\text{O}^+$ DR cross sections for full calculation (solid) and with only $v=0$ (dashed).

the full cross section. Above 0.0248 eV, the $v=0$ only cross section shows no structure and simply depicts direct recombination.

Fig. 5 is similar to Fig. 4 except that the dashed line is now for the case in which the $v=0$ and $v=1$ levels are included for the ion and Rydberg states. The dashed curve is now higher at the lowest energies than the dashed curve of Fig.4 due to the $v=1$ levels. Denoting the resonances as (v, n, Ω) , the peak in the dashed curve at 0.026 eV is the $(1, 9, \frac{1}{2})$ Rydberg resonance level. Note that in the full cross section, the same resonance is a dip due to interference with other states. The low energy wing of this resonance in the dashed curve raises the cross sections above those with only $v=0$ included. A $(1, 8, \frac{3}{2})$ Rydberg level lies mostly below threshold but has a wing that extends above threshold where it also affects the shape of the cross section. At energies above the $(1, 9, \frac{1}{2})$ level, there are three levels with peaks at 0.051 eV, 0.067 eV and 0.092 eV corresponding to $(1, 9, \frac{3}{2})$, $(1, 10, \frac{1}{2})$, and $(1, 10, \frac{3}{2})$ respectively. Except for the structure in the solid curve near 0.04 eV, each of the $v=1$ resonances listed in the prior sentence has a resonance in nearly the same position in the solid curve identifying these as $v=1$ resonances. The solid curve resonances all have a very different shape than the dashed curve resonances due to interference with other Rydberg levels. The $v=1$ resonances in the solid curve in Fig.5 are quite similar to those for

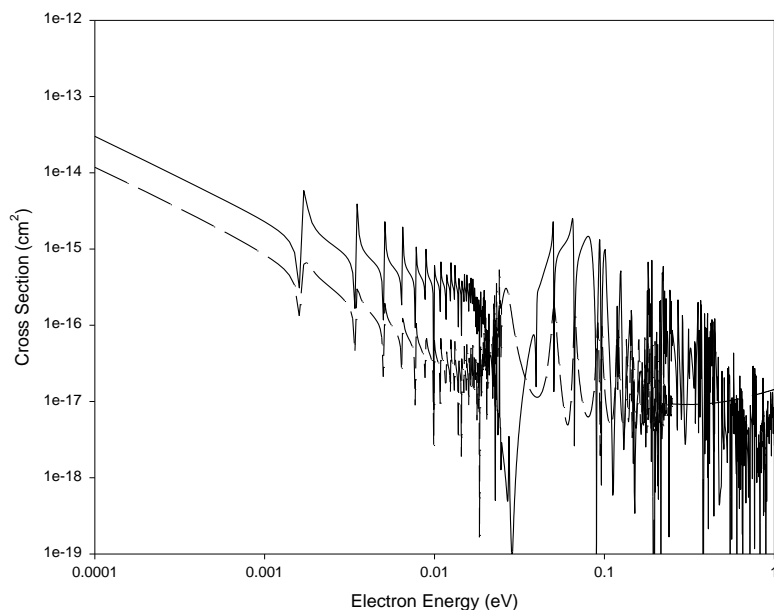


Figure 5. $^{18}\text{O}^{16}\text{O}^+$ DR cross sections for full calculation (solid) and with only $v=0-1$ (dashed).

$^{16}\text{O}_2^+$ except that they are shifted 0.0067 eV below the corresponding $^{16}\text{O}_2^+$ resonances due to the mass difference. Including resonance interference, the shift is estimated to be 0.0050-0.0067 eV. (See the two labeled $v=1$ resonances in Fig. 3). Neglecting the anharmonicities and higher terms, the energy of vibrational level v relative to $v=0$ is $E^{18,16}(v) = \omega^{18,16} v$ in $^{18}\text{O}^{16}\text{O}^+$ and $E^{16,16}(v) = \omega^{16,16} v$ in $^{16}\text{O}_2^+$. The difference is given by $\Delta E(v) = E^{16,16}(v) - E^{18,16}(v) = (\omega^{16,16} - \omega^{18,16}) v = 0.0067 v$ eV. Therefore, the mass difference causes large shifts of high v resonances and small shifts of low v resonances. Since high v resonances have low n , the electronic widths (which vary as n^{-3}) can be large.

Of the remaining vibrational levels, the largest changes in the cross section structure are due to $v=12$, $v=13$ and $v=14$. The addition of $v=12$ (Fig. 6) leads to a drop in the cross section by two orders of magnitude below 0.001 eV. Addition of the $v=13$ level raises the cross section below 0.001 eV by over an order of magnitude and some of the resonances between 0.03 and 0.1 resemble the full cross section resonances. Also, the large dip due in part to level $(1, 9, \frac{1}{2})$ falls at about 0.049 eV. With the addition of $v=14$, the $(1, 9, \frac{1}{2})$ dip moves closer to its final position at 0.029-0.027 eV. Cross sections including $v=15, 16$ and 17 closely agree with the full cross section calculated with 19 vibrational levels.

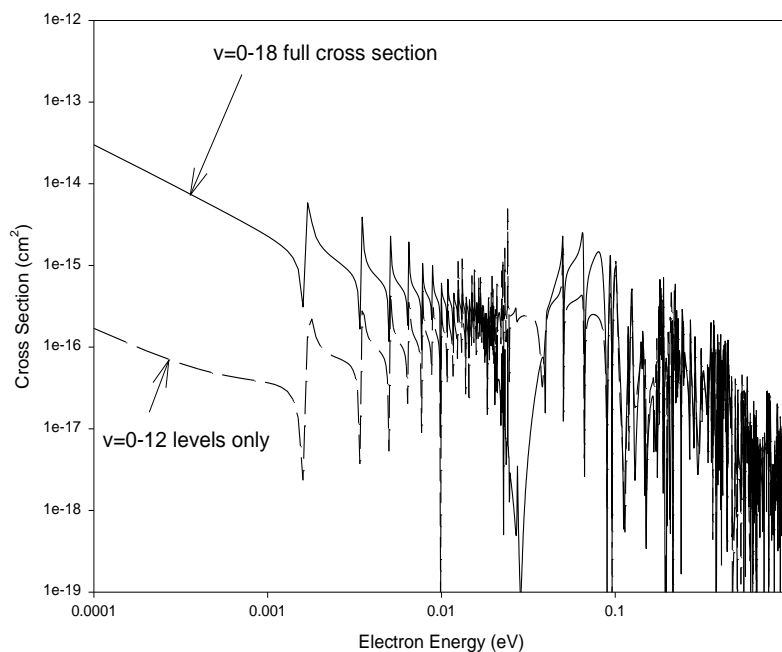


Figure 6. $^{18}\text{O}^{16}\text{O}^+$ DR cross sections for full calculation (solid) and with only $v=0-12$ (dashed).

5 Conclusions

The high v , low n resonances account for the differences between the $^{16}\text{O}_2^+$ and $^{18}\text{O}^{16}\text{O}^+$ cross sections and rate coefficients due to their large energy displacements and large electronic widths. The most important resonances are those with $n=3$ and $v=12, 13$, and 14 . If one considers only the mass difference, these resonances are shifted down in $^{18}\text{O}^{16}\text{O}^+$ relative to $^{16}\text{O}_2^+$ by $0.0067v$ eV. This shift is modified by resonance interference and for $v=1$ the calculated shift down is $0.0050-0.0067$ eV.

It is clear that one cannot use $^{18}\text{O}^{16}\text{O}^+$ experimentally determined cross sections and rate coefficients to accurately describe the DR of $^{16}\text{O}_2^+$. The high v low n resonances are expected to play an important role in determining the DR cross section structure in other molecular ions at $0.0-1.0$ eV electron energy. As a result, the conclusions reached here for O_2^+ are expected to apply to other molecular ions as well.

6 Acknowledgments

The research reported here is supported by NASA grants NAG5-6834 and NAG5-4286 and by the U.S. National Science Foundation (NSF) under grant ATM98-12034.

References

1. D. Kella, P. J. Johnson, H. B. Pedersen, L. Vejby-Christensen and L. H. Andersen, *Phys. Rev. Lett.* **77**, 2432 (1996).
2. D. Kella, L. Vejby-Christensen, P. J. Johnson, H. B. Pedersen, L. H. Andersen, *Science* **276**, 1530 (1997); *ibid.* **277**, 167 (1997).
3. The square brackets indicate that the basis functions are contracted, i.e. each consists of one or more primitive Gaussians. 5s denotes 5 s-type Gaussian contracted functions at each nucleus.
4. T. H. Dunning Jr., *J. Chem. Phys.* **90**, 1007 (1989).
5. H.-J. Werner and P. J. Knowles, *ibid.* **82**, 5053 (1985); P. J. Knowles and H.-J. Werner, *Chem. Phys. Lett.* **115**, 259 (1985).
6. H.-J. Werner and P. J. Knowles, *J. Chem. Phys.* **89**, 5803 (1988); P. J. Knowles and H.-J. Werner, *Chem. Phys. Lett.* **145**, 514 (1988).
7. MOLPRO is a package of ab initio programs written by H.-J. Werner and P. J. Knowles with contributions from J. Almlof, R. D. Amos, M. J. O. Deegan, S. T. Elbert, C. Hampel, W. Meyer, K. Peterson, R. Pitzer, A. J. Stone, P. R. Taylor and R. Lindh.
8. K. P. Huber and G. Herzberg, *Molecular Spectra and Molecular Structure, IV. Constants of Diatomic Molecules*, (Van Nostrand Reinhold Co., New York, 1979).
9. (a) S. L. Guberman, to be published (1999). (b) S. L. Guberman, Ab initio studies of Dissociative Recombination, in *Dissociative Recombination: Theory, Experiment, and Applications*, ed. By J. B. A. Mitchell and S. L. Guberman (World Scientific, Singapore, 1989), p.45.
10. A. Giusti, *J. Phys. B* **13**, 3867 (1980).
11. S. L. Guberman and A. Giusti-Suzor, *J. Chem. Phys.* **95**, 2602 (1991).
12. S. L. Guberman, *Science* **278**, 1276 (1997).
13. J. N. Bardsley, *J. Phys. B* **1**, 365 (1969).
14. S. L. Guberman, Potential Energy Curves for Dissociative Recombination, in *Physics of Ion-Ion and Electron-Ion Collisions* ed. by F. Brouillard (Plenum, New York, 1983) pp. 167-200.
15. E. A. Colbourn and A. E. Douglas, *J. Mol. Spectrosc.* **65**, 332 (1977).